Understanding Winter Precipitation Impacts on Automated Gauge Observations within a Real-Time System

STEVEN M. MARTINAITIS, STEPHEN B. COCKS, YOUCUN QI, AND BRIAN T. KANEY

Cooperative Institute for Mesoscale Meteorological Studies, University of Oklahoma, and NOAA/OAR National Severe Storms Laboratory, Norman, Oklahoma

JIAN ZHANG AND KENNETH HOWARD

NOAA/OAR National Severe Storms Laboratory, Norman, Oklahoma

(Manuscript received 27 January 2015, in final form 17 June 2015)

ABSTRACT

Precipitation gauge observations are routinely classified as ground truth and are utilized in the verification and calibration of radar-derived quantitative precipitation estimation (QPE). This study quantifies the challenges of utilizing automated hourly gauge networks to measure winter precipitation within the real-time Multi-Radar Multi-Sensor (MRMS) system from 1 October 2013 to 1 April 2014. Gauge observations were compared against gridded radar-derived QPE over the entire MRMS domain. Gauges that reported no precipitation were classified as potentially stuck in the MRMS system if collocated hourly QPE values indicated nonzero precipitation. The average number of potentially stuck gauge observations per hour doubled in environments defined by below-freezing surface wet-bulb temperatures, while the average number of observations when both the gauge and QPE reported precipitation decreased by 77%. Periods of significant winter precipitation impacts resulted in over a thousand stuck gauge observations, or over 10%–18% of all gauge observations across the MRMS domain, per hour. Partial winter impacts were observed prior to the gauges becoming stuck. Simultaneous postevent thaw and precipitation resulted in unreliable gauge values, which can introduce inaccurate bias correction factors when calibrating radar-derived QPE. The authors then describe a methodology to quality control (QC) gauge observations compromised by winter precipitation based on these results. A comparison of two gauge instrumentation types within the National Weather Service (NWS) Automated Surface Observing System (ASOS) network highlights the need for improved gauge instrumentation for more accurate liquid-equivalent values of winter precipitation.

1. Introduction

Accurate surface precipitation measurements from gauge networks are critical to flood and flash flood warning operations and to long-term seasonal and climatological assessments. These direct surface measurements are vital for modeling and verification of hydrometeorological prediction as well as for the calibration of remote sensing quantitative precipitation estimation (QPE). Precipitation gauge measurements are widely considered as ground truth; however, the point coverage of gauge networks lacks the spatial distribution needed for hydrometeorological operations and research, including situations where highly variable precipitation may not be accurately represented (e.g., Goodrich et al. 1995). In contrast, radar-derived QPE provides a high spatiotemporal resolution along with greater spatial coverage to capture the variabilities of precipitation distribution. Gauge observations are commonly used to calibrate radar-derived QPE, even though the sampling size between the gauge orifice and a typical radar pixel differs by approximately eight orders of magnitude (Droegemeier et al. 2000; Young et al. 2000). Gauges not vetted by a quality control (QC) procedure can negatively impact the calibration and statistical analysis and verification of radar-derived precipitation estimation (Steiner et al. 1999).

Challenges regarding precipitation gauge accuracy have been well documented. Blockages can result in

Corresponding author address: Steven M. Martinaitis, National Severe Storms Laboratory, 120 David L. Boren Blvd., Norman, OK 73072.
E-mail: steven.martinaitis@noaa.gov

DOI: 10.1175/JHM-D-15-0020.1

precipitation underestimation or even the prevention of measuring precipitation (Sevruk 2005; Sieck et al. 2007), while poor gauge siting can result in systematic biases (Sieck et al. 2007). Surface winds can lead to precipitation undercatch (Larson and Peck 1974; Wilson and Brandes 1979; Sevruk 1989; Essery and Wilcock 1991; Sevruk et al. 1991; Yang et al. 1998; Habib et al. 1999); however, strong winds can also cause equipment damage, power outages resulting in loss of automated data transmission, or even the evacuation of personnel in the case of manned sites (Martinaitis 2008). Loss of liquid or splash out during the tipping process, notably with intense rainfall rates, or double tipping can skew results with tipping-bucket gauge types (Parsons 1941). Mechanical malfunctions and telemetry and transmission issues resulting in report time inaccuracies, improper calibration, and evaporation can also impact gauge performance (Groisman and Legates 1994; Steiner et al. 1999; Marzen and Fuelberg 2005; Kondragunta and Shrestha 2006; Sieck et al. 2007).

Additional difficulties arise when gauges are tasked to measure winter precipitation. While some gauge types are capable of handling winter precipitation, the instrumentation can be subject to blockage of the gauge orifice or accumulation on the side of orifice walls (Goodison et al. 1998). Unmeasured accumulations collected on the gauge orifice are not recorded until falling into the bucket, usually after an increase of ambient air temperature (Goodison et al. 1998). Some tipping-bucket gauge networks utilize electrical heaters to melt solid precipitation for real-time measurement; however, increased evaporative loss of melted precipitation and enhanced sublimation of newly fallen snow have been observed (Metcalfe and Goodison 1992; Savina et al. 2012). Undercatch of snow can also occur with wetting losses on the internal walls of the gauge (Groisman and Legates 1994; Goodison et al. 1998).

Gauge instrumentation designed to measure the liquid equivalent of solid, winter precipitation are also subject to challenges regarding observational accuracy and efficiency. Automated gauges deemed capable of handling winter precipitation come in many gauge and windshield configurations (Nitu and Wong 2010) with varying collection efficiencies (Rasmussen et al. 2012). Environmental conditions have been shown to have a greater impact on snow measurements than that of rainfall measurements (Rasmussen et al. 2012). Automated gauge errors during snow events generally ranged from 20% to 50% because of the undercatch in windy conditions, while observed hourly catch efficiency of double Alter shielded gauges were greatly reduced in winds approaching $6\,\mathrm{m\,s^{-1}}$ (Rasmussen et al. 2012). Collection efficiency in windy conditions was found to be dependent upon snow crystal types and mass, degrees of riming and aggregation, varying turbulence intensity, and gauge geometry (Rasmussen et al. 2012; Thériault et al. 2012). Blowing snow and oscillatory motions of the weighing mechanism, also referred to as wind pumping, can also introduce errors with gauge measurements in windy conditions (Goodison et al. 1998). Evaporation and sublimation in relatively high ambient temperatures were also contributing factors to gauge losses during snow events (Metcalfe and Goodison 1993).

While radar-derived QPE can provide greater spatiotemporal coverage, it also has its own inherent set of limitations. Ground clutter, blockage, and nonmeteorological echoes can contaminate the lowest elevation scans (Young et al. 1999; Harrison et al. 2000). Greater beam sampling volume with increasing radar range reduces spatial resolution of QPE and introduces inhomogeneous beam filling (Steiner et al. 1999). The radar beam can undersample precipitation by overshooting precipitation features at far distances because of the curvature of Earth (Smith et al. 1996; Steiner et al. 1999). Melting layer effects can result in bright banding, leading to erroneously high precipitation estimates (Smith 1986; Anagnostou and Krajewski 1998; Klazura et al. 1999). Radar QPE products are also subject to improper calibration and limited operational reflectivity–rain rate (Z–R) relationships (Smith et al. 1996; Young et al. 1999; VanCleve and Fuelberg 2007). Operational relationships between radar reflectivity and liquid-equivalent snowfall rate (Z–S) have been shown to be highly variable and provide great uncertainty with radar-derived QPE due to differing snowfall properties (Passarelli 1978; Rasmussen et al. 2003).

Other sampling limitations can introduce spatial and temporal uncertainties with estimating winter precipitation. Slow, yet highly variable, fall speeds of snow (Thériault et al. 2012) can introduce significant elapsed time between radar detection aloft and surface gauge detection, notably at the onset of an event. Even when winter precipitation reached the surface, Savina et al. (2012) observed an average delay of 30.2 min in recording the beginning of a snow event using a tipping-bucket gauge with a heating element. This temporal difference was attributed to melting the precipitation, filling the first tip, and evaporative losses. Horizontal advection of hydrometeors can introduce geographical discrepancies of up to tens of kilometers between radar-measured precipitation and surface observations with far sampling ranges from radar (e.g., Lauri et al. 2012).

The Multi-Radar Multi-Sensor (MRMS) QPE system (hereinafter denoted as Q3) utilizes an overlapping network of radars and automated gauge networks across the continental United States (CONUS) and southern

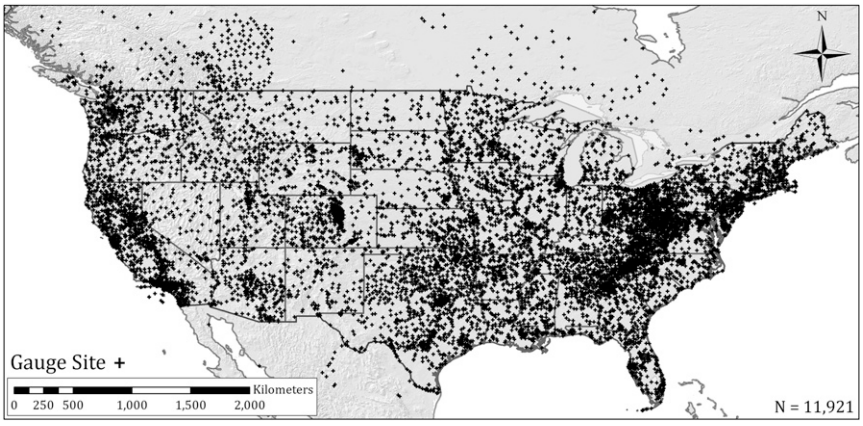

FIG. 1. Location of all gauge sites ingested by MRMS during the study period.

Canada to generate seamless, high spatiotemporal QPE mosaics (Zhang et al. 2011). Gauge observations that pass a QC procedure are utilized in the local bias correction and verification of mosaicked radar-derived QPE, as well as the generation of gridded gauge-based QPE. Since multisensor QPE products are dependent upon the application of gauge observations to improve radar-based precipitation accumulations, the impacts of winter precipitation on the ability of gauges to measure precipitation can yield misrepresentative local bias correction values. A better understanding is required on the commonality of adverse winter precipitation impacts to automated gauge networks within real-time QPE generation. This study will investigate and quantify winter precipitation impacts on gauges through gauge versus radar QPE comparisons in Q3. Potential precipitation detection errors include stuck observations, impacts of winter precipitation prior to the gauges becoming stuck, and postevent thaw behavior. The findings will be utilized in addressing real-time mitigation strategies in the MRMS gauge QC logic.

2. Data and methodology

The automated, real-time hourly gauge data ingested by MRMS from 0000 UTC 1 October 2013 to 0000 UTC 1 April 2014 from a total of 11 921 gauge sites were examined across the MRMS domain (Fig. 1). Gauge data were obtained from the National Centers for Environmental Prediction (NCEP), the National Operational Hydrologic Remote Sensing Center (NOHRSC), and the Oklahoma Climatological Survey (OCS) Mesonet. Gauge networks provided by NCEP and NOHRSC included the National Weather Service (NWS) Hydrometeorological Automated Data System (HADS) network, the Automated Surface Observing System (ASOS), and other local and regional automated networks through the Meteorological Assimilation Data Ingest System (MADIS). These gauge networks utilize a variety of instrumentation types and configurations (Table 1); however, they are not well documented between all network sources and not distinguished in the MRMS system. Approximately 40 million nonmissing hourly gauge observations of accumulated water content were considered during the study period.

Hourly gauge observations were compared to collocated 1 km × 1 km gridded radar-only Q3 (Q3RAD) accumulations of instantaneous precipitation rates aggregated over each hour (Zhang et al. 2011). Q3RAD is derived from a two-dimensional (2D) seamless hybrid scan reflectivity (SHSR) mosaic where the

TABLE 1. Description of the gauge instrumentation types and configurations from each network ingested by MRMS. The ASOS network is separated between HTB and AWPAG weighing gauges. The HADS and MADIS networks are operated by various agencies with a variety of gauge configurations. The measurement sensitivity is 0.25 mm.

Gauge source	Gauge type	Shielding	Heating element
HADS	Multiple gauge instrumentation configurations		
ASOS HTB	30-cm tipping bucket	Vinyl alter style	Yes
ASOS AWPAG	Weighing	Tretyakov or double Alter style	No (antifreeze)
OCS	30-cm tipping bucket	Alter style	No
MADIS	Multiple gauge instrumentation configurations		

TABLE 2. Periods of significant winter weather impacts on gauge observations. Each event was defined as at least 16 consecutive hours with 500 or more gauge vs radar comparisons per hour classified as $G = 0, R > 0$ in an environment characterized by RAP model surface $T_{wb} \leq 0.00°C$. Listed in this table are the start time and date of the periods of significant winter precipitation impacts, the number of consecutive hours, and the average percent of nonmissing gauge observations per hour that are within an environment characterized by RAP model surface $T_{wb} \leq 0.00°C$.

Event No.	Period start time and date			Consecutive hours	Percent observations for RAP surface $T_{wb} \leq 0.00°C$
	Time (UTC)	Date	Year		
1	2000	25 Nov	2013	17	72.9%
2	1500	5 Dec	2013	40	63.4%
3	0300	8 Dec	2013	23	79.4%
4	0100	14 Dec	2013	25	64.5%
5	2200	1 Jan	2014	35	77.9%
6	0900	21 Jan	2014	19	91.2%
7	0900	25 Jan	2014	17	88.9%
8	0600	28 Jan	2014	29	88.0%
9	0400	31 Jan	2014	16	77.4%
10	0800	4 Feb	2014	33	70.1%
11	0300	8 Feb	2014	19	76.3%
12	0900	12 Feb	2014	40	75.2%
13	1500	15 Feb	2014	20	75.9%
14	0900	17 Feb	2014	27	69.9%
15	0700	2 Mar	2014	39	64.2%
16	2200	16 Mar	2014	17	68.3%

instantaneous surface precipitation rate (SPR) is calculated from the SHSR and surface precipitation type (SPT) classification, which allows for a unique Z–R relationship to be applied at each grid cell. Spherical, gridded radar data used in the generation of MRMS products are interpolated onto a three-dimensional (3D) Cartesian grid utilizing a nearest-neighbor mapping approach on the range–azimuth plane and an exponential weighting interpolation in the elevation direction (Zhang et al. 2005; Lakshmanan et al. 2006). The mosaicked 2D SHSR utilized in Q3RAD is generated from a weighted, nearest-neighbor approach of single-radar SHSR where the data with the lowest elevation receive the greatest contribution to each grid cell (Zhang et al. 2011). The instantaneous SPR for precipitation classified as snow in the MRMS system is generated using the following Z–R relationship:

$$Z = 75R^{2.0}. \quad (1)$$

A minimum reflectivity threshold of 5 dBZ results in a minimum detectable rate for snow in Q3RAD of approximately 0.25 mm (0.01 in.), which matches the minimum reporting value of gauge observations utilized in this study. Hour-long accumulations of SPR values along with the minimum reflectivity threshold help reduce the impact of potential partial beam filling with MRMS products.

Analysis between Q3RAD and gauge accumulations was conducted on the hourly time scale at the top of each hour, since the gauge-based MRMS products are generated at that temporal resolution. Comparisons between hourly gauge observations G and hourly Q3RAD rate accumulations R were assigned one of four classifications: both gauge and Q3RAD reporting no precipitation (G, $R = 0$), both gauge and Q3RAD reporting precipitation (G, $R > 0$), gauge reporting precipitation but Q3RAD does not ($G > 0$, $R = 0$), and Q3RAD reporting precipitation but the gauge does not ($G = 0, R > 0$). Events classified as $G, R = 0$ were excluded from the analysis. A radar quality index (RQI; Zhang et al. 2012) was used to ensure that

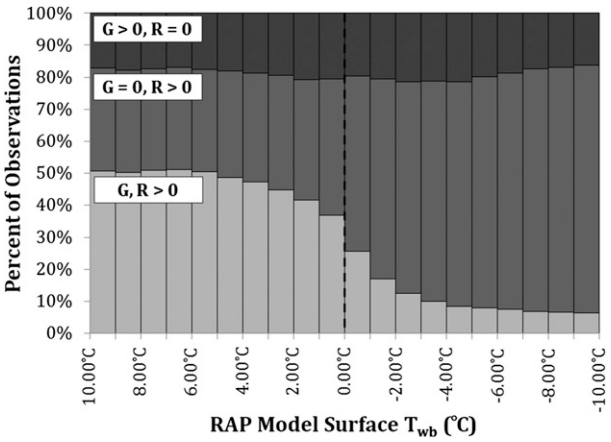

FIG. 2. Histogram of the percentage of hourly gauge vs Q3RAD classification types for sites where RQI ≥ 0.1 and for RAP model surface T_{wb} from −10.00° to 10.00°C. The G, $R = 0$ classification was excluded. The vertical dashed line in the histogram represents RAP model surface $T_{wb} = 0.00°C$.

TABLE 3. Distribution of gauge vs Q3RAD comparison classifications for the entire study period in areas where RQI ≥ 0.1 and for when RAP model surface $T_{wb} > 0.00°$ and ≤ 0.00°C. The $G, R = 0$ classification was excluded from this analysis. The sample size of the number of hourly gauge observations is also listed in this table.

RAP model surface T_{wb}	$G, R > 0$	$G = 0, R > 0$	$G > 0, R = 0$	N
>0.00°C	46.9%	33.9%	19.2%	2 485 628
≤0.00°C	10.6%	62.5%	26.9%	1 863 953

gauge versus Q3RAD pairings were in areas of adequate radar data quality and coverage, as defined by the MRMS system. The RQI product is derived from radar sampling characteristics related to beam blockage, beamwidth, and beam sampling relationships with respect to the freezing level. A nonzero RQI value (i.e., RQI ≥ 0.1) would indicate that the radar is sampling precipitation and is less than 50% blocked. Gauge sites that were in regions where RQI ≥ 0.1 and had less than 10% of its observations denoted as missing were utilized in more detailed G, R analysis.

The gauge versus Q3RAD comparison classifications were assessed against hourly surface wet-bulb temperature T_{wb} values derived from the Rapid Refresh (RAP) model on the MRMS 1 km × 1 km Cartesian grid. Utilizing surface T_{wb} accounted for the occurrence of winter precipitation within environments characterized by above-freezing ambient temperatures and nonsaturated relative humidity values (e.g., Matsuo and Sasyo 1981). Surface T_{wb} values were generated from the RAP model, since not all gauge data ingested and decoded in real time by the MRMS system contained additional environmental

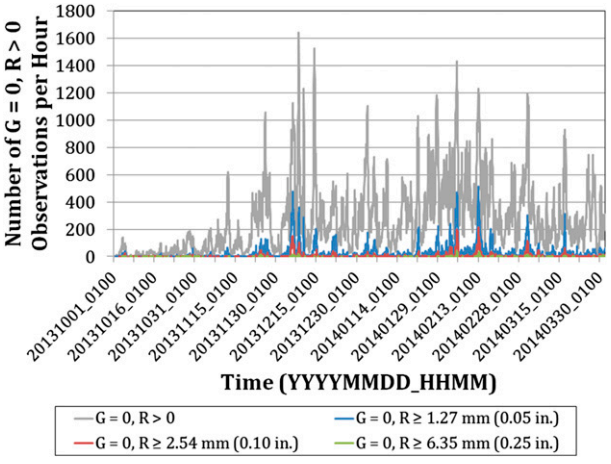

FIG. 3. Number of $G = 0$, $R > 0$ observations per hour within environments characterized by RAP model surface $T_{wb} \leq 0.00°C$ (gray) and for Q3RAD values of at least 1.27 (blue), 2.54 (red), and 6.35 mm (green).

information to generate observed T_{wb} at each gauge site. Although biases can exist with model-derived surface T_{wb}, the use of the model-derived gridded MRMS surface T_{wb} product allows for a surface T_{wb} value to be assessed at all gauge sites. An RAP model surface T_{wb} of 0.00°C was employed as a method to delineate between surface environments conducive for liquid precipitation types and solid, winter precipitation types. An unknown percentage of these $G = 0$, $R > 0$ events in RAP model surface $T_{wb} \leq 0.00°C$ regimes could be a result of false light precipitation generated within Q3RAD or from potential spatiotemporal discontinuities between Q3RAD and gauge observations in winter precipitation. These unknowns cannot be distinguished within the automated,

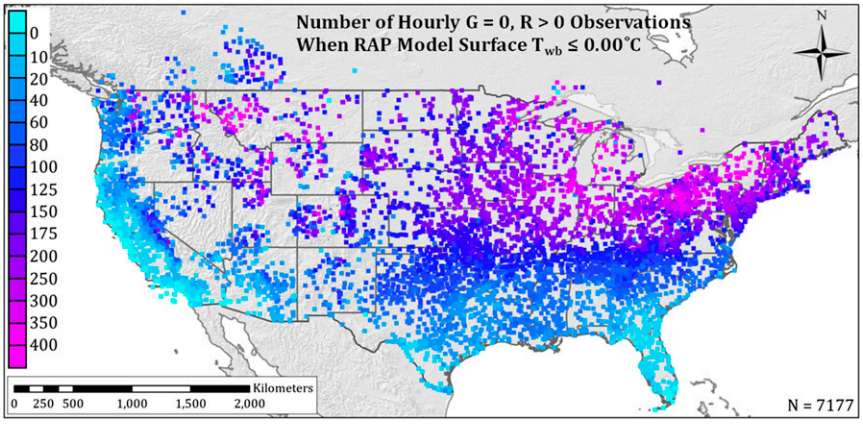

FIG. 4. Number of $G = 0$, $R > 0$ observations per hour when RAP model surface $T_{wb} \leq 0.00°C$ at each gauge site over the MRMS domain. Gauge sites shown had at least 90% data availability with an average RQI ≥ 0.1 over the study period.

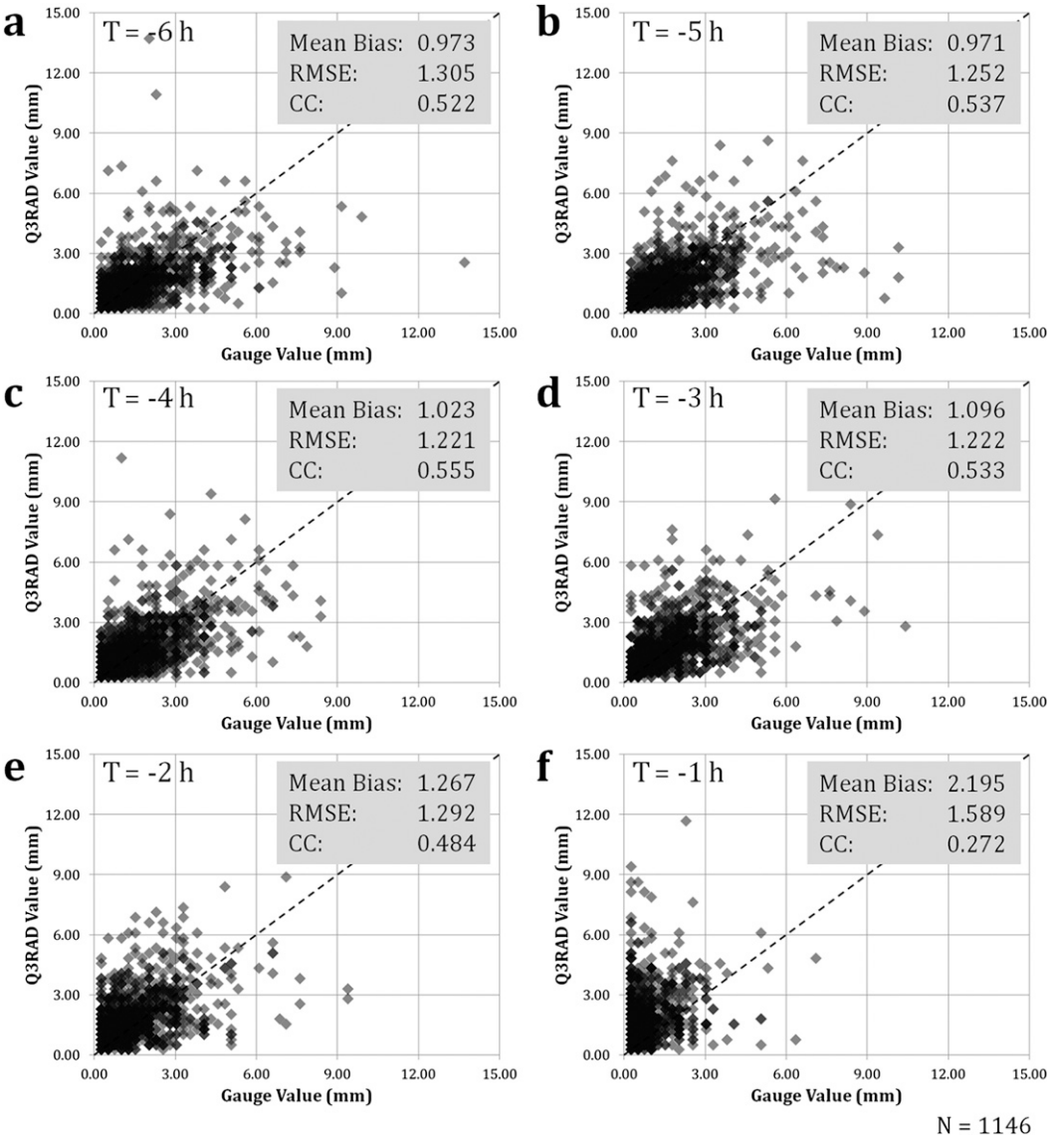

FIG. 5. Scatterplot of Q3RAD vs gauge observations prior to becoming stuck from (a) $T = -6$ h to (f) $T = -1$ h. The dashed line represents the one-to-one line between gauge and Q3RAD values. Statistical evaluations of each hour prior to becoming stuck are located in the upper-right corner of (a)–(f). The sample size of the number of gauge vs Q3RAD observations is denoted at the lower-right corner of (f).

real-time MRMS system; thus, all $G = 0$, $R > 0$ observations were retained in this study.

Gauge observations were also examined prior to becoming stuck via statistical comparisons to the collocated Q3RAD from 2 h after the gauge was characterized as stuck ($T = 2$ h) to 6 h prior ($T = -6$ h). Both the gauge and collocated Q3RAD product had to record nonzero values from $T = -6$ h to $T = -1$ h and then meet the $G = 0$, $R > 0$ criteria within an RAP model surface $T_{wb} \leq 0.00$°C environment starting at $T = 0$ h. The 2-h period for the $G = 0$, $R > 0$ values was used to mitigate precipitation event termination at $T = 0$ h. There were 1146 8-h periods of gauge and Q3RAD observations that met the aforementioned criteria. Quantitative evaluations between the gauge observations and Q3RAD values for winter precipitation impacts were assessed using the following statistics: mean bias ratio, root-mean-square error (RMSE), and the Pearson linear correlation coefficient (CC), where

$$\text{mean bias} = \frac{\sum_{i=1}^{N} R_i}{\sum_{i=1}^{N} G_i}, \tag{2}$$

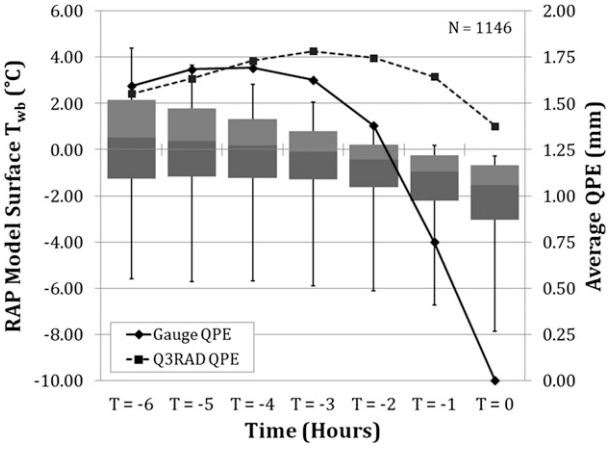

FIG. 6. Box-and-whisker plot of RAP model surface T_{wb} with line graph of average gauge and Q3RAD values from $T = -6$ h to $T = 0$ h. The upper (lower) part of each box represents the 75th (25th) percentile with the line in the middle of each box representing the median RAP model surface T_{wb}. The upper (lower) whisker represents the 90th (10th) percentile. The solid black line with diamond markers (dashed dark gray line with square markers) represents the average gauge (Q3RAD) value for each time. The sample size of 6-h periods of gauge and Q3RAD observations is denoted at the upper-right corner.

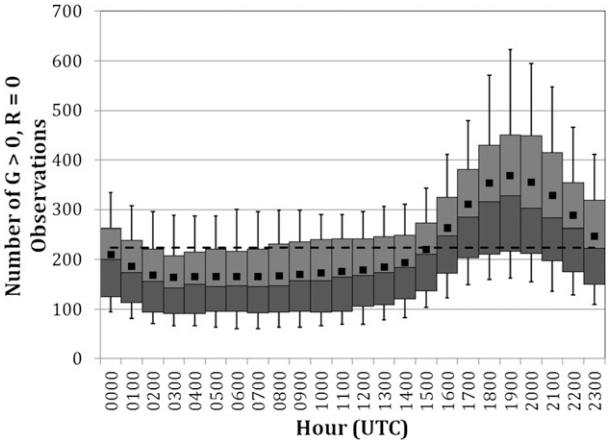

FIG. 7. Box-and-whisker plot of number of $G > 0$, $R = 0$ observations vs time of day (UTC). The upper (lower) part of each box represents the 75th (25th) percentile with the line in the middle of each box representing the median value. The upper (lower) whisker represents the 90th (10th) percentile. The black dot represents the mean number of $G > 0$, $R = 0$ observations for each hour, and the dashed line represents the overall mean number of $G > 0$, $R = 0$ observations.

$$\mathrm{RMSE} = \sqrt{\frac{1}{N}\sum_{i=1}^{N}(R_i - G_i)^2}, \quad \text{and} \tag{3}$$

$$\mathrm{CC} = \frac{\mathrm{cov}(R, G)}{\sigma_R \sigma_G}. \tag{4}$$

The total number of comparisons N is dependent upon the nonmissing gauge and Q3RAD observations. For CC, cov refers to the covariance, and σ is the standard deviation. Analysis of hourly gauge observations and Q3RAD values were also conducted for periods of significant winter precipitation impacts on gauge observations (Table 2), which was defined as at least 16 consecutive hours with 500 or more gauge versus radar comparisons per hour classified as $G = 0$, $R > 0$ in an environment characterized by RAP model surface $T_{wb} \leq 0.00$°C.

3. Examination of winter precipitation impacts

a. Complete loss of gauge observations

Gauge versus Q3RAD comparisons that contained at least one nonzero observation exhibited two distinct sets of results based on RAP model surface T_{wb} values. Figure 2 represents the distribution of the gauge versus Q3RAD comparisons as a function of RAP model surface T_{wb}. Events identified as G, $R > 0$ were the dominant classification for the above-freezing RAP model surface T_{wb}. In contrast, the $G = 0$, $R > 0$ classification was observed most often in below-freezing T_{wb} environments. Events classified as G, $R > 0$ accounted for 46.9% of the gauge versus Q3RAD comparisons when RAP model surface $T_{wb} > 0.00$°C, while $G = 0$, $R > 0$ classifications accounted for 33.9% of the observations (Table 3). The percent of G, $R > 0$ events reduced from 46.9% to 10.6% when RAP model surface $T_{wb} \leq 0.00$°C, which was approximately a 77% reduction in the quantity of G, $R > 0$ observations to an average of 45 G, $R > 0$ observations per hour. The percent of $G = 0$, $R > 0$ observations rose to approximately 62.5% or an average of 267 observations per hour. The significant increase in $G = 0$, $R > 0$ classifications along with the decrease in G, $R > 0$ classifications was likely due to the gauges becoming impacted by winter precipitation. The $G > 0$, $R = 0$ classification accounted for an average of 19% of the observations across the RAP model surface T_{wb} distribution. The $G > 0$, $R = 0$ observations are a result of either postevent thawing of accumulated winter precipitation or a false observation unrelated to winter weather impacts. There was no relationship found between the distribution of $G > 0$, $R = 0$ observations and surface T_{wb}.

Figure 3 displays a time series of the number of $G = 0$, $R > 0$ observations per hour, stratified by precipitation totals, when the RAP model surface $T_{wb} \leq 0.00$°C. There were 11 periods totaling 102 h that resulted in at least 1000 observations classified as $G = 0$, $R > 0$ per hour. The majority of $G = 0$, $R > 0$ events were when

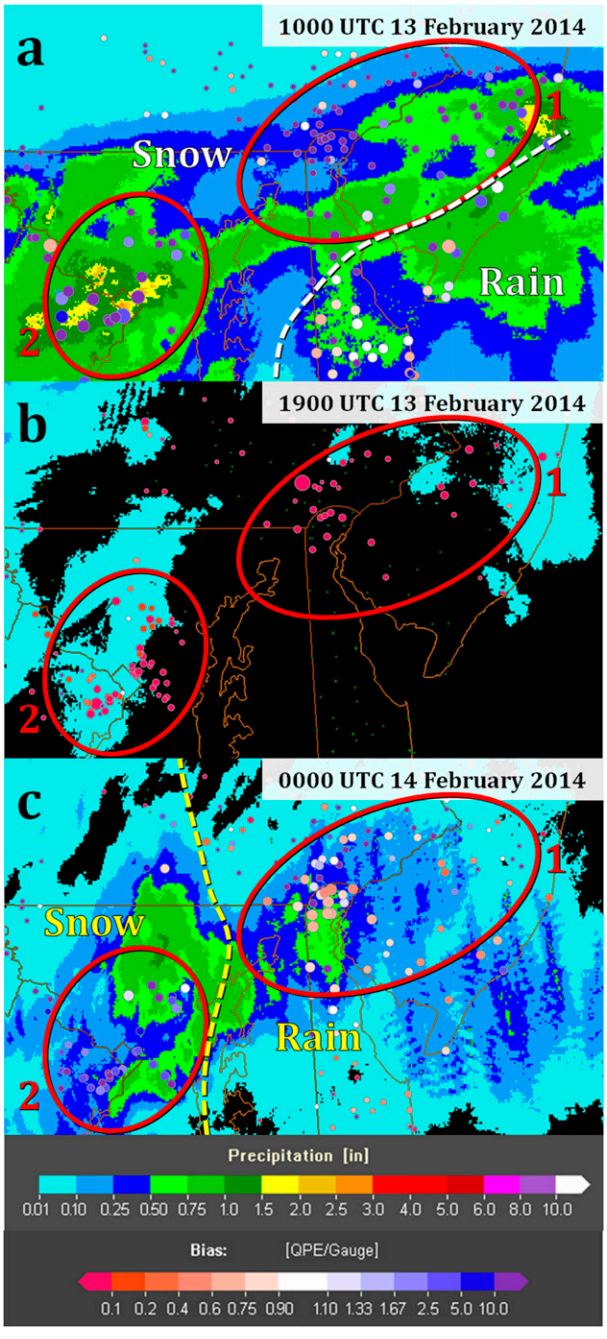

FIG. 8. Precipitation and thawing event sequence at (a) 1000 UTC 13 Feb 2014, (b) 1900 UTC 13 Feb 2014, and (c) 0000 UTC 14 Feb 2014. Q3RAD is shown in color fill (in.) and gauge observations with bias value are shown in colored bubble plot. Areas of snow and rain that occurred at times in (a) and (c) are delineated by white and yellow dashed lines, respectively. Regions 1 and 2 (denoted by red circles) are used in the statistical analysis shown in Fig. 9. Region 1 (2) had stuck gauges from winter precipitation [in (a)] followed by rain (snow) after thawing commenced [in (c)].

hourly Q3RAD was less than 1.27 mm (0.05 in.), where an unknown quantity of these observations could be related to winter weather sampling challenges; however, gauge observations classified as $G = 0$, $R > 0$ were also found in regions experiencing moderate to heavy, solid winter precipitation that resulted in Q3RAD values exceeding 12.7 mm (0.50 in.). There were 291 h when there were at least 100 observations classified as $G = 0$, $R \geq 1.27$ mm (0.05 in.) and 29 h when there were at least 100 observations classified as $G = 0$, $R \geq 2.54$ mm (0.10 in.). Only 435 h during the study period had stuck gauges in areas where $R \geq 6.38$ mm (0.25 in.).

Spatial coverage of the number of hourly observations when $G = 0$, $R > 0$ in an RAP model surface $T_{wb} \leq 0.00$°C environment showed the majority of potentially stuck gauge observations extended from the middle Mississippi River Valley to New England and within the mountainous western United States (Fig. 4). Gauge sites in these locations totaled over 300 h of $G = 0$, $R > 0$ observations during the study period. The $G = 0$, $R > 0$ observations were rather infrequent along the Pacific coast and the southeastern United States, where less than 20 total $G = 0$, $R > 0$ h were observed.

b. *Gauge observation quality before becoming stuck*

Scatterplots between hourly gauge observations and their collocated Q3RAD hourly values indicated diminished gauge performance prior to becoming stuck (Fig. 5). A mean bias ratio near 1.00 was observed from $T = -6$ h through $T = -3$ h, followed by a notable bias increase to 2.195 by $T = -1$ h. The increase in the mean bias ratio would generally signify an overestimation by the Q3RAD product, but this change in the mean bias ratio would likely be attributed to partial winter weather impacts on the gauge instrumentation. The RMSE remained near constant from 1.22 to 1.31 mm throughout the period up to $T = -2$ h, followed by an increase in the RMSE to 1.589 mm by $T = -1$ h. The CC also remained steady from $T = -6$ h to $T = -3$ h, with an ensuing degradation of CC to 0.272 at $T = -1$ h. The low CC values throughout the evaluated time period could be related to the given uncertainty in both gauge observations in winter precipitation and radar-estimated liquid water equivalents.

Figure 6 demonstrates the change in average hourly gauge and Q3RAD values with respect to time and RAP model surface T_{wb}. The average gauge and Q3RAD hourly values were above 1.50 mm (0.06 in.) from $T = -6$ h to $T = -3$ h. The average gauge observation decreased from 1.69 mm (0.067 in.) at $T = -4$ h to 0.75 mm (0.030 in.) by $T = -1$ h before becoming stuck at $T = 0$ h. The

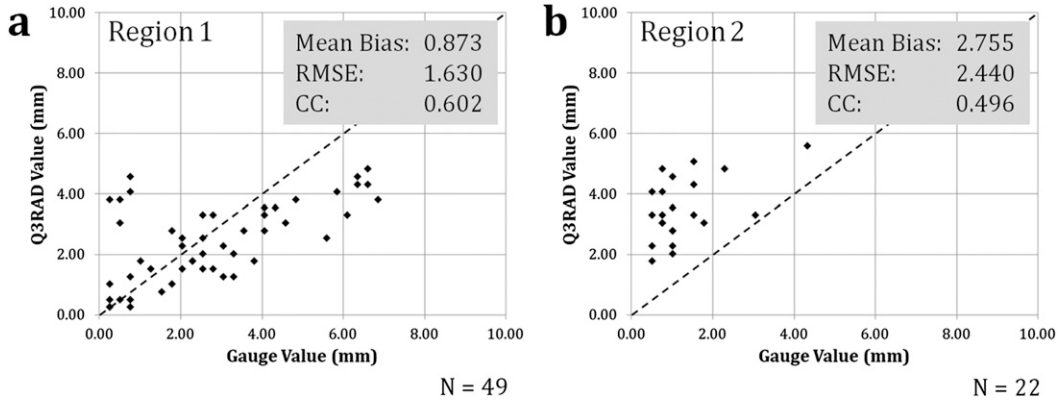

FIG. 9. Scatterplot of Q3RAD vs gauge observations at 0000 UTC 14 Feb 2014 for (a) region 1 and (b) region 2 highlighted in Fig. 8. The dashed line represents the one-to-one line between gauge and Q3RAD values. Statistical evaluation of the mean bias ratio, RMSE (mm), and CC for each region are located in the upper-right corner of (a) and (b). The sample size for each region is denoted at the lower-right corner of (a) and (b).

average Q3RAD value at these gauge sites remained above 1.64 mm (0.064 in.) from $T = -5$ h to $T = -1$ h with a slight decrease to an average of 1.38 mm (0.054 in) at $T = 0$. The duration that a stuck gauge was located within a favorable winter precipitation environment prior to recording a $G = 0$, $R > 0$ observation ranged from less than 1 to 6 h or more. Approximately 37% of the observations at $T = -6$ h were in environments characterized by the RAP model surface $T_{wb} \leq 0.00$°C. The percentage of gauge observations in environments conducive for winter precipitation steadily increased to 85% by $T = -1$ h. It could be assumed that gauge sites can be partially impacted for a varying range of time before completely losing their capability for measuring winter precipitation. Therefore, the quality of the G, $R > 0$ observation when RAP model surface $T_{wb} \leq 0.00$°C would have to be considered as suspect in an automated, real-time system.

c. *Postevent thawing*

A second, yet equally important impact is the post-event thawing of accumulated winter precipitation on

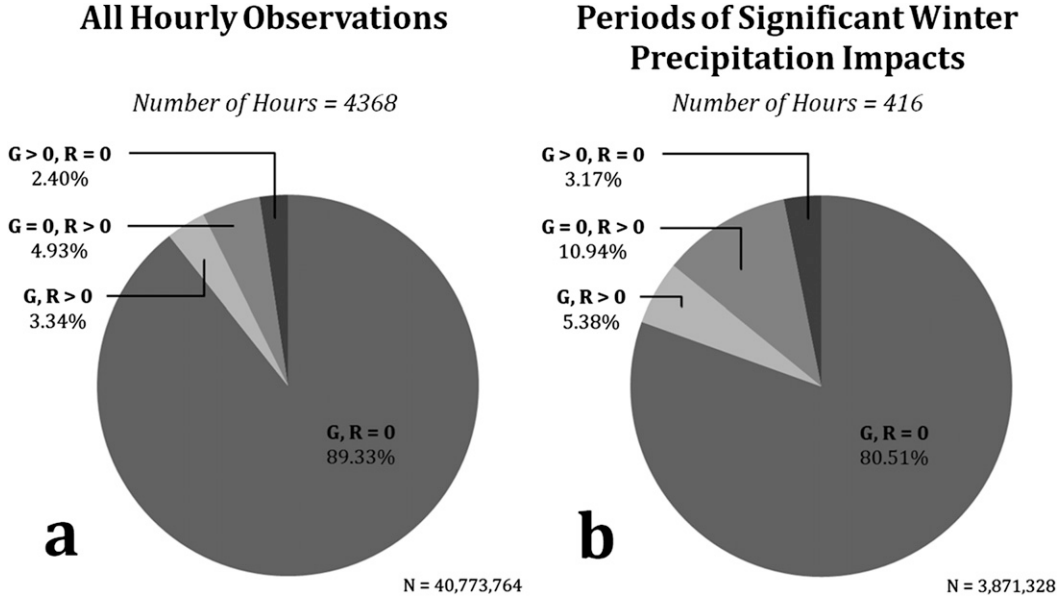

FIG. 10. Distribution of all gauge vs Q3RAD comparison classifications for (a) the entire study period and (b) periods of significant winter precipitation impacts. The number of hours for each analysis is denoted above the pie chart. The sample size of the number of hourly G, R pairings is denoted at the lower-right corner of (a) and (b).

TABLE 4. Evaluation of the max number of impacted hours during and after periods of significant winter weather impacts on gauge observations defined in Table 2. Listed in this table regarding stuck gauges are the max number of $G = 0$, $R > 0$ observations per hour when RAP model surface $T_{wb} \leq 0.00°C$; the max percent of all observations per hour that were $G = 0$, $R > 0$ when RAP model surface $T_{wb} \leq 0.00°C$; and the average percent of $G = 0$, $R > 0$ observations that were in an environment characterized by RAP model surface $T_{wb} \leq 0.00°C$. Listed in this table regarding postevent thawing are the max number of $G > 0$, $R = 0$ observations per hour and the max percent of all observations characterized as $G > 0$, $R = 0$ per hour.

	$G = 0$, $R > 0$ observations when $T_{wb} \leq 0.00°C$			$G > 0$, $R = 0$ observations	
Event No.	Max number per hour	Max percent per hour	Percent of all $G = 0$, $R > 0$ observations	Max number per hour	Max percent of all observations
1	1060	11.6%	75.6%	561	5.9%
2	1126	11.9%	73.1%	476	5.0%
3	1644	17.6%	90.0%	967	11.1%
4	1529	16.1%	68.4%	548	5.6%
5	1103	11.4%	74.8%	519	5.4%
6	1034	10.8%	92.7%	213	2.3%
7	896	10.9%	98.3%	237	2.6%
8	1186	12.5%	92.0%	711	7.6%
9	707	7.4%	85.2%	850	8.8%
10	1435	14.9%	88.6%	569	6.0%
11	845	8.6%	77.7%	722	7.4%
12	1232	12.9%	84.7%	1187	12.2%
13	800	8.3%	75.6%	470	4.9%
14	862	9.1%	87.8%	632	6.7%
15	1194	12.4%	83.7%	1619	16.5%
16	930	9.5%	69.6%	532	5.4%

gauges. Melting from increased surface ambient temperature or solar radiation resulted in gauges reporting nonzero hourly observations during nonprecipitation periods. Figure 7 displays the average number of $G > 0$, $R = 0$ observations versus time of day. Less than 170 observations per hour were observed as $G > 0$, $R = 0$ between 0200 and 0800 UTC; however, an average of over 300 observations per hour met this classification between 1700 and 2100 UTC. The peak hour for maximum $G = 0$, $R > 0$ observations was 1900 UTC, which had an average of 369 gauge observations meeting the $G = 0$, $R > 0$ classification and a 90th percentile value of 623 gauge observations. It is understood that an unknown quantity of gauge sites per hour reported nonzero observations due to technical or other nonhydrometeorological reasons; however, the 220% increase of $G > 0$, $R = 0$ observations during peak diurnal heating and solar radiation would strongly indicate the presence of thawing winter precipitation.

Identifying thawing impacts became increasingly complex when coinciding with additional precipitation. An example of this occurred over a portion of the mid-Atlantic region on 13–14 February 2014 (Fig. 8). Winter precipitation was observed across the example domain except for southern Delaware and southern New Jersey. Gauges located in New Jersey, northern Delaware, and far southeastern Pennsylvania (region 1) along with the area around the District of Columbia (region 2) had become partially or completely stuck by 1000 UTC 13 February (Fig. 8a) from winter precipitation. As the precipitation moved northward out of the domain, thawing commenced with above-freezing ambient surface temperatures (Fig. 8b). Average liquid values accumulating in the gauges from thawing were 1–3 mm h^{-1} in both regions. Additional precipitation commenced during this thawing period, with rain (snow) primarily being observed over region 1 (region 2) by 0000 UTC 14 February based on surface observations (Fig. 8c).

The inherent issue with additional precipitation simultaneously occurring during the thawing of accumulated solid precipitation is that the gauge observational quality becomes compromised. The scatterplot of the gauge versus Q3RAD values within region 1 depicted what would appear as an underestimation by the Q3RAD product with a mean bias ratio of 0.873 (Fig. 9a). A more likely scenario is that automated gauges were accumulating the melt from previous precipitation combined with the current rainfall. In contrast, the scatterplot and resulting mean bias ratio of 2.755 for region 2 would assume a significant Q3RAD overestimation (Fig. 9b).

TABLE 5. As in Table 3, but for periods of significant winter precipitation impacts.

RAP model surface T_{wb}	$G, R > 0$	$G = 0, R > 0$	$G > 0, R = 0$	N
>0.00°C	53.0%	26.9%	20.1%	290 381
≤0.00°C	11.7%	74.5%	13.8%	464 316

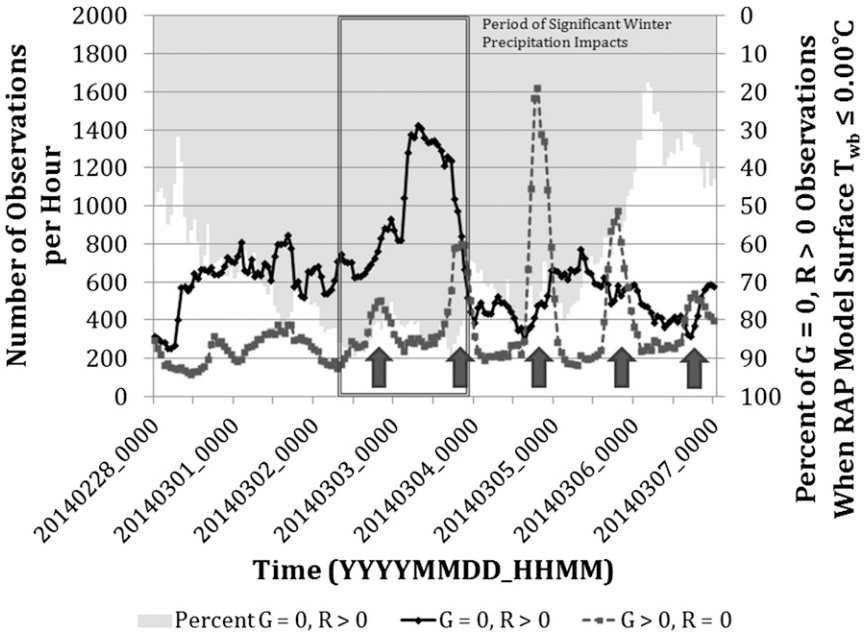

FIG. 11. Evaluation of all $G = 0, R > 0$ and $G > 0, R = 0$ comparisons from 0000 UTC 28 Feb to 0000 UTC 7 Mar 2014. The percent of $G = 0$, $R > 0$ observations in environments characterized by RAP model surface $T_{wb} \leq 0.00$°C is depicted by the bar graph (light gray). The period of significant winter precipitation impacts on gauges (event 15 from Table 2) is denoted by the gray box. Dark gray arrows highlight periods of thawing during diurnal heating based on $G > 0$, $R = 0$ (dark gray dashed line) line graph.

Gauge behavior in region 2 better resembled continued thawing with little to no new accumulating winter precipitation being sampled due to a blocked gauge orifice.

d. Significant winter precipitation impacts analysis

There were 16 periods classified as having significant winter precipitation impacts on gauge observations (Table 2). These periods of significant winter precipitation impacts encompassed 416 h or less than 10% of the study period. For any given hour during the study period, 89.33% of the observations were G, $R = 0$ (Fig. 10a). The other 10.67% of the observations were composed of the other gauge versus Q3RAD classifications where at least one sensor reported a

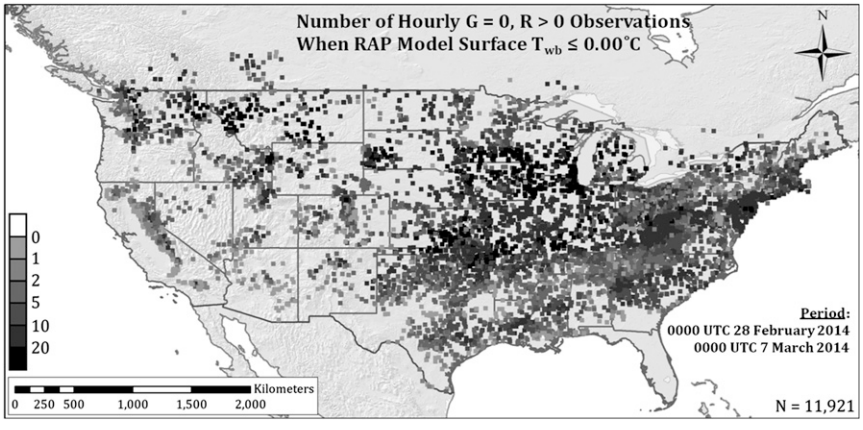

FIG. 12. Number of hourly $G = 0, R > 0$ observations when RAP model surface $T_{wb} \leq 0.00$°C and RQI ≥ 0.1 at each gauge site from 0000 UTC 28 Feb to 0000 UTC 7 Mar 2014. Gauge sites that recorded zero hours that met the aforementioned criteria were not displayed. The gauge sites with at least one $G = 0, R > 0$ hourly observation displayed represent 65.9% of the gauges ingested by Q3.

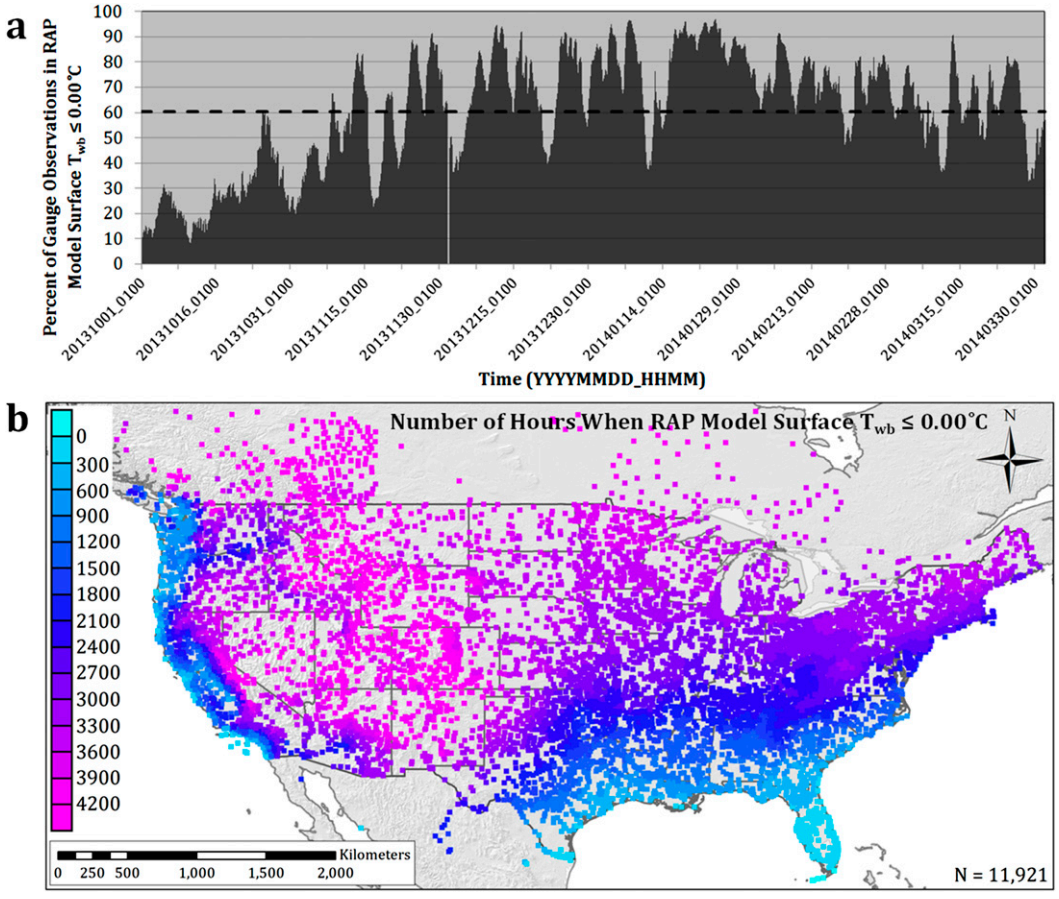

FIG. 13. (a) Bar graph of the percent of gauge sites per hour located within an environment characterized by RAP model surface $T_{wb} \leq 0.00°C$. The dashed line represents the average percentage of gauge sites per hour in an environment of RAP model surface $T_{wb} \leq 0.00°C$ over the study period. (b) The number of hours at each gauge site when the RAP model surface $T_{wb} \leq 0.00°C$.

nonzero precipitation value. Periods of significant winter precipitation impacts had an average of 19.49% of observations per hour with at least one sensor reporting a nonzero value (Fig. 10b). The greatest contributor to this increased number of G, R classifications with at least one nonzero observation during periods of significant winter precipitation impacts was the more than doubling of the average number of $G = 0$, $R > 0$ classifications per hour from 4.93% of all G, R pairings to 10.94% during the periods of significant winter precipitation impacts. This translated to an average of 1018 $G = 0$, $R > 0$ observations per hour during those 416 h regardless of RAP model surface T_{wb}.

Ten of the periods of significant winter precipitation impacts had at least 1 h with over 1000 gauges characterized as $G = 0$, $R > 0$ in areas where RAP model surface $T_{wb} \leq 0.00°C$ (Table 4). Event 3 had a maximum of 1644 $G = 0$, $R > 0$ observations in 1 h, which accounted for 17.6% of all nonmissing gauge observations. Most $G = 0$, $R > 0$ observations during the periods of significant winter precipitation impacts occurred in environments defined by RAP model surface $T_{wb} \leq 0.00°C$. The proportion of gauge versus Q3RAD classifications based on RAP model surface T_{wb} were similar to the average hour during the study period, but the $G = 0$, $R > 0$ classification encompassed a greater percentage and quantity of observations when the RAP model surface $T_{wb} \leq 0.00°C$ (Table 5). These periods of significant winter precipitation impacts were followed by an increase in warm ambient temperatures and solar radiation, such as events 12 and 15, that resulted in a large quantity of $G > 0$, $R = 0$ observations per hour from potential thawing under clear air (Table 4). Closely spaced winter precipitation events and those with prolonged below-freezing ambient temperatures, such as events 6–8, had a relatively smaller number of gauges reporting potential postevent thaw per hour.

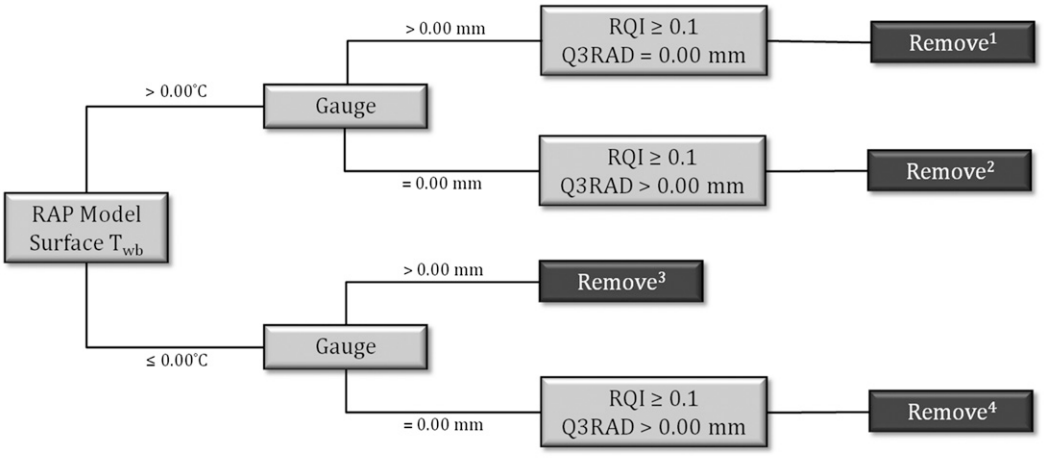

[1] Removes gauges that are recording false precipitation observations, including post-event thaw
[2] Removes gauges that are recording false zero observations not related to winter precipitation impacts
[3] Removes gauges to mitigate winter precipitation impacts on non-zero gauge observations regardless of RQI or Q3RAD QPE. This includes gauges that are recording false precipitation observations (i.e., G > 0, R = 0), including post-event thaw.
[4] Removes gauges that are recording false zero observations likely related to winter precipitation impacts

FIG. 14. Subsection of Q3 gauge QC logic related to identification and removal of gauge observations impacted by winter precipitation and postevent thawing.

Figure 11 shows the evolution of all $G = 0, R > 0$ and $G > 0, R = 0$ observations during a 1-week period beginning at 0000 UTC 28 February 2014. A 39-h period of significant winter precipitation impacts on gauges occurred during this week (event 15 from Table 2). Approximately 83.7% of $G = 0, R > 0$ observations, which totaled up to a maximum of 1194 $G = 0, R > 0$ observations per hour, were located in environments defined by the RAP model surface $T_{wb} \leq 0.00$°C during the classified period of significant winter weather impacts (Table 4). A pronounced diurnal cycle of thawing based on $G > 0, R = 0$ observations was identified as early as 2 March 2014. Peak thawing occurred at 1900 UTC 4 March 2014 with 1619 $G > 0, R = 0$ observations. The overall extent of the winter weather during the 1-week period starting at 0000 UTC 28 February 2014 potentially impacted an estimated 65.9% of the gauge sites ingested by MRMS based on the reporting of at least one $G = 0, R > 0$ observation in environments defined by RAP model surface $T_{wb} \leq 0.00$°C and when RQI ≥ 0.1 (Fig. 12). Approximately 25.6% of gauge sites had at least 10 h of observations that were considered as stuck (i.e., $G = 0, R > 0$), while 6.0% of gauge sites had at least 20 hourly observations that were considered stuck.

4. Discussion on gauge quality control

a. Impacts and quality control

The substantial quantity of gauge observations per hour identified as potentially impacted by winter precipitation within the MRMS system poses a number of challenges with automated multisensor QPE generation. Figure 13a shows the percent of gauge observations that were located in areas when RAP model surface $T_{wb} \leq 0.00$°C. On average, 60.4% of gauge observations per hour were in environments conducive for winter precipitation types. The average gauge site in the MRMS domain spends approximately 2066 h in the below-freezing RAP model surface T_{wb} (Fig. 13b). New England, the Great Lakes region, the central and northern plains, and the majority of the western United States had over 3000 h of below-freezing RAP model surface T_{wb} values. The number of below-freezing surface T_{wb} hours exceeded 4000 in the Rocky Mountains. In contrast, the far southeastern United States, notably along the Gulf Coast, and the Pacific coast had between 0 and 600 h of RAP model surface $T_{wb} \leq 0.00$°C. Despite the large spatial variability, surface environments favorable for winter precipitation types and subsequent gauge impacts were quite common during the study period.

The MRMS gauge QC algorithm was modified to remove all nonzero gauge values when the RAP model surface $T_{wb} \leq 0.00$°C and RQI ≥ 0.1 (Fig. 14). The gauge QC scheme also removes all $G = 0, R > 0$ classifications regardless of RAP model surface T_{wb} values; thus, this logic will account for the potentially stuck gauges that can occur. While this scheme could remove an unknown number of relatively accurate observations, the gauge QC algorithm effectively removes problematic gauge

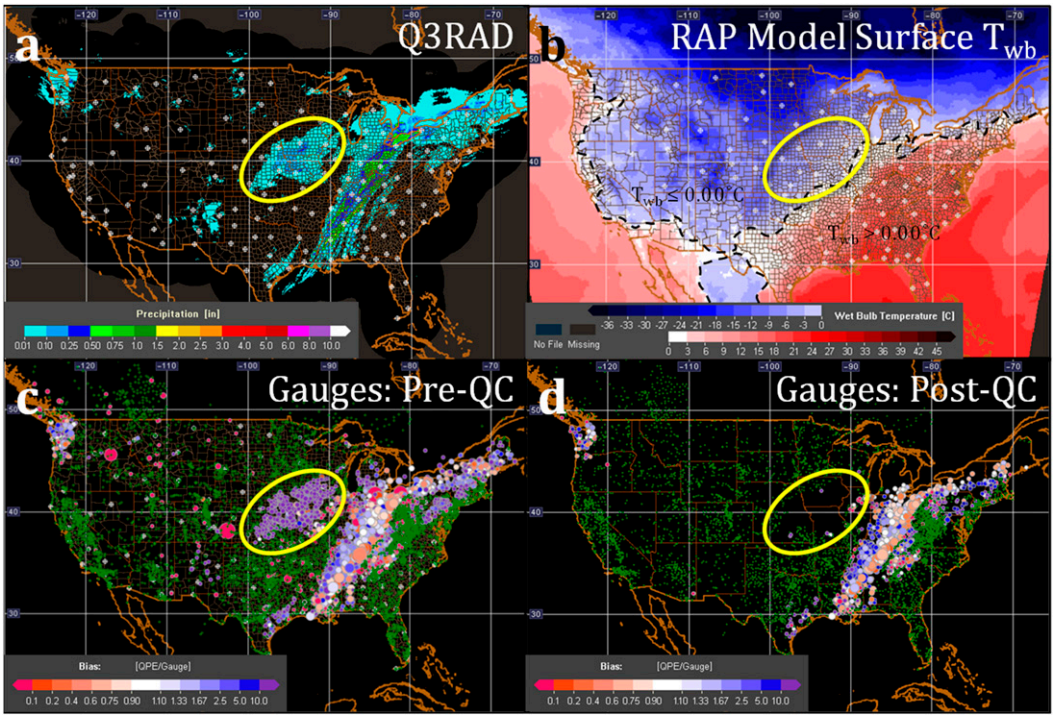

FIG. 15. Observations at 0600 UTC 22 Dec 2013 of (a) hourly Q3RAD (in.), (b) RAP model surface T_{wb} (°C) with black dashed line denoting $T_{wb} = 0.00$°C, (c) gauges prior to QC, and (d) gauges after application of QC. The yellow circle highlights a region of stuck gauges from winter precipitation in a region characterized by RAP model surface $T_{wb} \leq 0.00$°C. Gauge bubble plots in (c) and (d) are based on bias ratio (color) and QPE amount (size). Gauge sites with $G, R = 0$ observations are denoted by green crosses. Corresponding color scales are located at the lower-left corner of (a)–(d).

observations likely compromised by winter precipitation. An example of how the gauge QC algorithm removes gauges impacted by winter precipitation is shown in Fig. 15. The highlighted area from southern Kansas to eastern Iowa experienced snowfall with hourly Q3RAD values of 1–4 mm (Fig. 15a) in a region of RAP model surface T_{wb} values from −2° to −10°C (Fig. 15b). Most gauges in the region were considered as stuck (Fig. 15c). Other gauges reported nonzero hourly observations, but those observations were considered suspect. The post-QC plot showed that all of the aforementioned gauges were removed from the highlighted region (Fig. 15d).

Figure 16 shows the difference in the local gauge-corrected Q3 (Q3GC) before and after the implementation of the winter precipitation QC logic during a snow event over an accumulation period of 24 h ending at 1200 UTC 6 January 2015. Both versions of the Q3GC product were compared against independent daily gauge observations from the Community Collaborative Rain, Hail and Snow (CoCoRaHS) network (Cifelli et al. 2005). The reduced quality of hourly gauge values was shown to have an adverse effect on the bias correction of the radar data (Figs. 16a,b) when compared to the Q3GC version with the hourly gauges removed from the bias correction process (Figs. 16c,d). The retaining of gauges during this winter event produced a mean bias ratio of 0.294 with an RMSE of 3.810 mm and a CC of 0.531. When all gauges in the area of winter precipitation were removed through the new QC logic, the mean bias ratio became closer to one to one, while the RMSE was reduced by half and the CC increased to 0.824.

Hourly gauge observations classified as $G > 0, R = 0$ are also removed through the gauge QC algorithm regardless of RAP model surface T_{wb} (Fig. 14). The removal of all $G > 0$, $R = 0$ events encompasses the nonzero gauge observations related to postevent thaw of solid precipitation in clear air environments. In contrast, a combination of thawing with concurrent precipitation cannot be readily identified and would yield an erroneous ground truth. Such inaccurate gauge values would introduce an improper bias correction ratio to local gauge-corrected QPE products. It is unknown how often this concurrent thawing and precipitation situation occurs, and there is currently no manual or

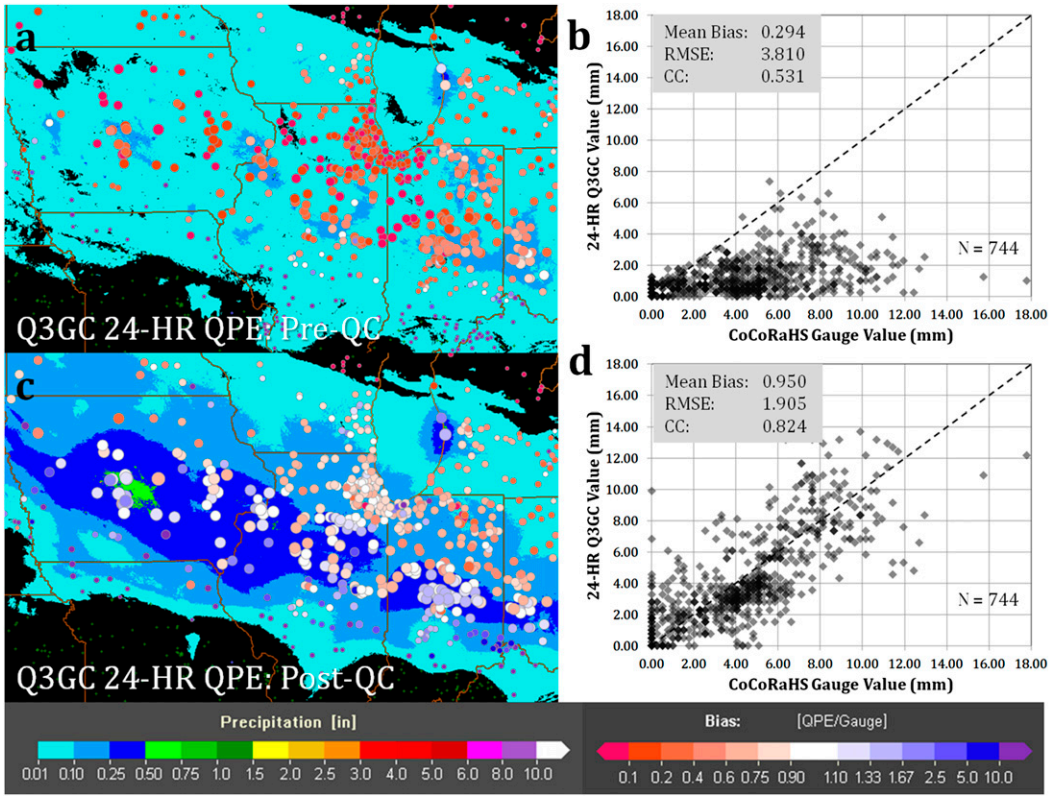

FIG. 16. Bubble plot of CoCoRaHS daily gauge observations with 24-h accumulation of Q3GC (in.) ending at 1200 UTC 6 Jan 2015 (a) prior to winter QC logic and (c) using the winter QC logic for gauges. Also shown is the scatterplot of Q3RAD vs CoCoRaHS observations at 1200 UTC 6 Jan 2015 (b) prior to winter QC logic and (d) using the winter QC logic for gauges. The dashed line represents the one-to-one line between CoCoRaHS and Q3GC values. Statistical evaluation of the mean bias ratio, RMSE (mm), and CC for each 24-h period are located in the upper-left corner of (b) and (d). The sample size for each region is denoted at the lower-right corner of (b) and (d).

automated method to extract liquid postevent thaw from concurrent new precipitation.

b. Improvements to gauge networks

Despite the challenges of erroneous gauge observations during winter precipitation events, a recent instrumentation upgrade of a subset of the ASOS network demonstrated some improved skill with measuring the liquid equivalent of winter precipitation. The ASOS network contains two series of gauge configurations: 1) the standard heated tipping bucket (HTB) and 2) the all-weather precipitation accumulation gauge (AWPAG). A network of 331 ASOS AWPAGs has been installed in the United States, Puerto Rico, Guam, and Saipan, with 303 ASOS AWPAGs located within the MRMS domain (Fig. 17). The ASOS AWPAG was developed to improve performance of measuring winter precipitation over the standard HTB (White et al. 2004; Greeney et al. 2005). Greeney et al. (2005) conducted a side-by-side comparison of the HTB and AWPAG configurations during the 2003/04 winter season in Sterling, Virginia, and Johnston, Pennsylvania. Hourly observations found the AWPAG instrumentation to be more compliant during winter and mixed precipitation events.

Evaluation of ASOS HTB and AWPAG observations ingested by MRMS exhibited similar performance in environments conducive for liquid precipitation defined by RAP model surface $T_{wb} > 0.00°C$ (Figs. 18a,c); however, the number of $G = 0$, $R > 0$ observations in environments supportive of winter precipitation types were reduced from 65.6% with HTB gauges (Fig. 18b) to 42.2% with AWPAGs (Fig. 18d). There were also more hourly G, $R > 0$ observations with AWPAGs. ASOS HTB gauges reported an average of 107 h of $G = 0$, $R > 0$ observations in conditions defined by RAP model surface $T_{wb} \leq 0.00°C$, while AWPAGs reported an average of 73 h of $G = 0$, $R > 0$ observations (Fig. 19). In contrast, the HTB gauges averaged 43 h of G, $R > 0$ observations in RAP model surface $T_{wb} \leq 0.00°C$

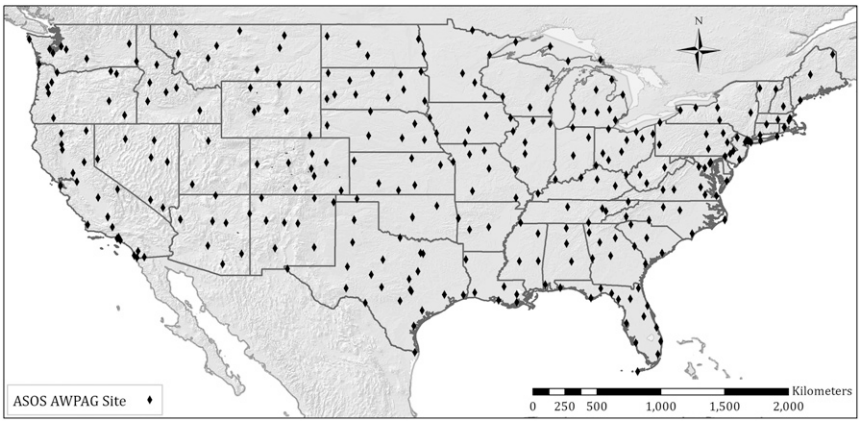

FIG. 17. Location of ASOS AWPAG sites across the CONUS.

environments, while the AWPAGs averaged 62 h of G, $R > 0$ observations.

A lack of accurate liquid-equivalent measurements of winter precipitation types introduces great uncertainties in QPE accumulations and is detrimental to both short-term operational needs and long-term climatological assessments. The current configuration of Q3 utilizes only radar and gauge networks to supply precipitation

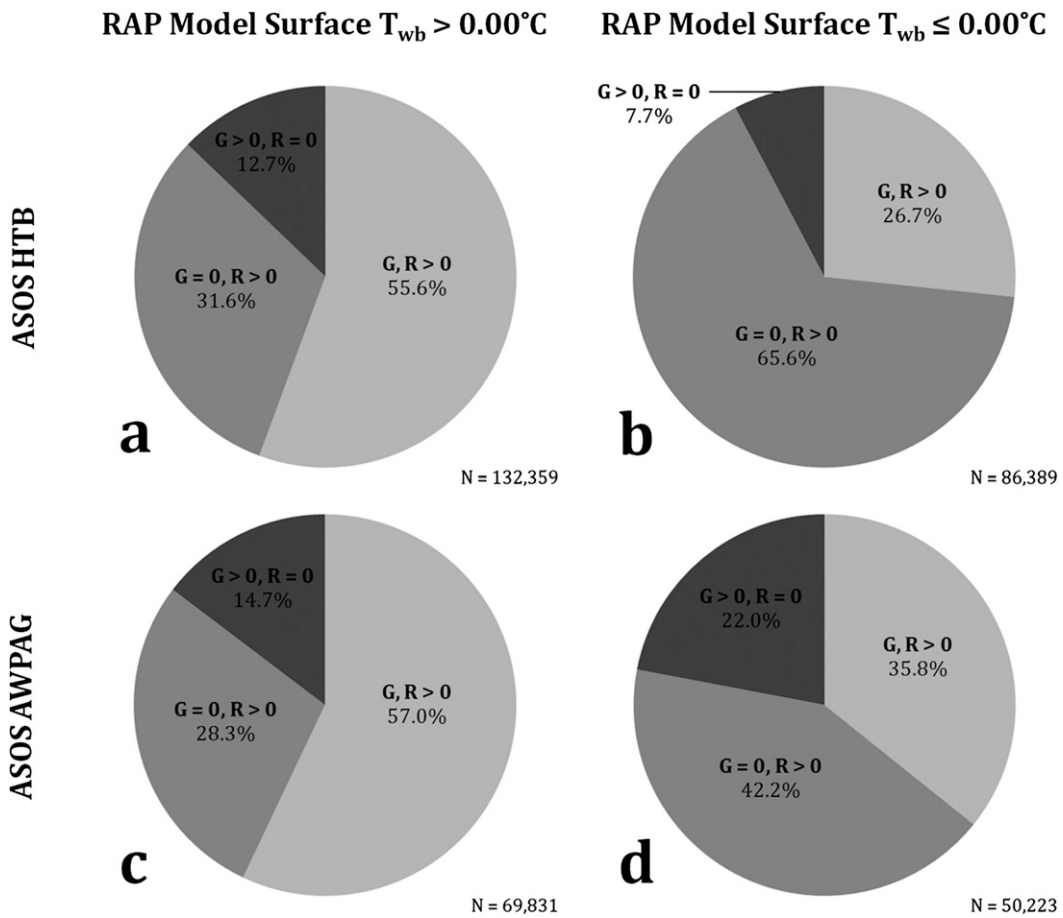

FIG. 18. Percentage of hourly comparison classification type between gauges and Q3RAD for the (a),(b) standard ASOS HTB sites and the (c),(d) ASOS AWPAG sites for when (left) RAP model surface $T_{wb} > 0.00°C$ and (right) RAP model surface $T_{wb} \leq 0.00°C$. The classification type $G, R = 0$ was excluded. The sample size is denoted at the lower-right corner of (a)–(d).

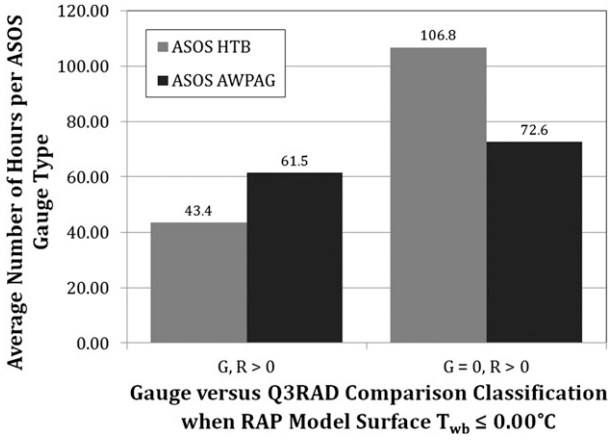

FIG. 19. Average number of hourly $G, R > 0$ and $G = 0, R > 0$ observation classifications for ASOS HTB (light gray) and ASOS AWPAG (dark gray) gauge types in environments characterized by RAP model surface $T_{wb} \leq 0.00°C$.

estimates. Given the large quantity of impacted gauges per hour and gauge QC logic, Q3 values are solely based on radar-only estimates in areas receiving winter precipitation. One of the greatest departures between an applied Z–R or Z–S relationship and a reference reflectivity rate QPE distribution along with the greatest level of QPE uncertainty was with the precipitation classified as snow (Kirstetter et al. 2015). The accuracy of hourly radar-derived QPE values of winter precipitation is unknown, since there is insufficient ground truth of liquid-equivalent precipitation values on the hourly scale. The majority of automated gauge networks utilize the HTB with varying windshield configurations. While HTB gauges are relatively cost-efficient, numerous studies have demonstrated that HTB instrumentation lacks meaningful skill in measuring snow and other winter precipitation types (Greeney et al. 2005; Rasmussen et al. 2012). Efforts are underway to examine the reliability of solid precipitation measurements through gauge intercomparisons and historical analysis (e.g., Rasmussen et al. 2012).

5. Summary

The operational objective of Q3 is to create accurate, high spatiotemporal resolution QPE. Q3 currently utilizes a network of overlapping radars and automated hourly precipitation gauge observations to generate QPE products in real time. While gauge observations are considered as ground truth and are used in local radar bias corrections, they have difficulties measuring winter precipitation. One such difficulty is winter precipitation adversely impacting the gauge instrumentation, such as blocking the gauge orifice or accumulating on the side of the orifice walls; thus, gauges likely report inaccurate observations during and after a winter precipitation event. This study quantifies the challenges of winter precipitation impacts on hourly gauge observations that were ingested by the Q3 automated real-time system and provides a straightforward QC methodology for removing gauges impacted by winter precipitation.

Gauge observations located in RAP model surface environments favorable for winter precipitation types had approximately 6 times more stuck observations (i.e., $G = 0, R > 0$) than $G, R > 0$ observations. Large winter storms traversing the MRMS domain would yield over 1000 stuck gauge observations per hour. Areas that observed winter precipitation more frequently averaged over 300 hourly $G = 0, R > 0$ observations per gauge site during the 6-month study period, while areas with more mild winter climates averaged less than 20 h of potentially stuck observations per site. The quality of gauge observations was also shown to diminish an average of 2 h prior to becoming stuck. A secondary impact from stuck gauges was postevent thawing with increased ambient temperatures and solar radiation. While thawing can be easily identified under clear air conditions, gauges measuring postevent thaw when simultaneously precipitating are not readily identified and would result in erroneous observations. These data can result in improper verification and calibration of radar-based QPE.

Specific logic was included in the Q3 gauge QC algorithm to remove gauges potentially impacted by winter precipitation based on this study. Gauge values in environments characterized by RAP model surface $T_{wb} \leq 0.00°C$ were removed if they were considered as stuck or partially impacted by winter precipitation. The QC algorithm also removed gauges that are classified as $G > 0$, $R = 0$ that are likely related to postevent thawing of accumulated winter precipitation on the gauge instrumentation; however, there is currently no methodology to exclude hourly gauge values that concurrently measured thaw and precipitation. The implementation of the new gauge QC logic mitigates the adverse impact of winter precipitation on gauge observations utilized in the local bias correction of radar-based QPE.

The ongoing challenge with the generation and QC of accurate hourly liquid-equivalent accumulations is the high degree of uncertainty in both gauge observations and radar-derived values. Further refinements to improve the MRMS gauge QC scheme in areas of winter precipitation and regions of reduced radar coverage are being investigated. This includes identifying specific gauge instrumentation types and configurations that can potentially be retained through a stringent QC process for QPE generation, local bias correction, and

verification. Future studies related to radar sampling and uncertainties of liquid water–equivalent values in Q3RAD, including a physically based methodology for further mitigation of potential false light precipitation, are ongoing.

Acknowledgments. The authors thank the anonymous reviewers for their comments and assistance. The authors also thank Dr. Chris Fiebrich from the Oklahoma Climatological Survey for his insight and review. Funding was provided by NOAA/Office of Oceanic and Atmospheric Research under NOAA–University of Oklahoma Cooperative Agreement NA11OAR4320072, U.S. Department of Commerce.

REFERENCES

Anagnostou, E. N., and W. F. Krajewski, 1998: Calibration of the WSR-88D precipitation processing subsystem. *Wea. Forecasting*, **13**, 396–406, doi:10.1175/1520-0434(1998)013<0396:COTWPP>2.0.CO;2.

Cifelli, R., N. Doesken, P. Kennedy, L. D. Carey, S. A. Rutledge, C. Gimmestad, and T. Depue, 2005: The Community Collaborative Rain, Hail, and Snow Network: Informal education for scientists and citizens. *Bull. Amer. Meteor. Soc.*, **86**, 1069–1077, doi:10.1175/BAMS-86-8-1069.

Droegemeier, K. K., and Coauthors, 2000: Hydrological aspects of weather prediction and flood warnings: Report on the ninth prospectus development team of the U.S. Weather Research Program. *Bull. Amer. Meteor. Soc.*, **81**, 2665–2680, doi:10.1175/1520-0477(2000)081<2665:HAOWPA>2.3.CO;2.

Essery, C. I., and D. N. Wilcock, 1991: Variation in rainfall catch from standard U.K. meteorological office raingauges. *Hydrol. Sci. J.*, **36**, 23–24, doi:10.1080/02626669109492482.

Goodison, B. E., P. Y. T. Louie, and D. Yang, 1998: WMO solid precipitation measurement intercomparison. WMO Instruments and Observing Methods Rep. 67, WMO/TD-872, 212 pp.

Goodrich, D. C., J.-M. Faures, D. A. Woolhiser, L. J. Lane, and S. Sorooshian, 1995: Measurement and analysis of small-scale convective storm rainfall variability. *J. Hydrol.*, **173**, 283–308, doi:10.1016/0022-1694(95)02703-R.

Greeney, C. M., M. D. Gifford, and M. L. Salyards, 2005: Winter test of production all-weather precipitation accumulation gauge for ASOS 2003–2004. *Ninth Symp. on Integrated Observing and Assimilation Systems for the Atmosphere, Oceans, and Land Surface (IOAS-AOLS)*, San Diego, CA, Amer. Meteor. Soc., 8.3. [Available online at https://ams.confex.com/ams/Annual2005/techprogram/paper_82895.htm.]

Groisman, P. Ya., and D. R. Legates, 1994: The accuracy of United States precipitation data. *Bull. Amer. Meteor. Soc.*, **75**, 215–227, doi:10.1175/1520-0477(1994)075<0215:TAOUSP>2.0.CO;2.

Habib, E., W. F. Krajewski, V. Nespor, and A. Kruger, 1999: Numerical simulation studies of rain gauge data correction due to wind effect. *J. Geophys. Res.*, **104**, 19 723–19 733, doi:10.1029/1999JD900228.

Harrison, D. L., S. J. Driscoll, and M. Kitchen, 2000: Improving precipitation estimates from weather radar using quality control and correction techniques. *Meteor. Appl.*, **7**, 135–144, doi:10.1017/S1350482700001468.

Kirstetter, P.-E., J. J. Gourley, Y. Hong, J. Zhang, S. Moazamigoodarzi, C. Langston, and A. Arthur, 2015: Probabilistic precipitation rate estimates with ground-based radar networks. *Water Resour. Res.*, **51**, 1422–1442, doi:10.1002/2014WR015672.

Klazura, G. E., J. M. Thomale, D. S. Kelly, and P. Jendrowski, 1999: A comparison of NEXRAD WSR-88D radar estimates of rain accumulation with gauge measurements for high- and low-reflectivity horizontal gradient precipitation events. *J. Atmos. Oceanic Technol.*, **16**, 1842–1850, doi:10.1175/1520-0426(1999)016<1842:ACONWR>2.0.CO;2.

Kondragunta, C., and K. Shrestha, 2006: Automated real-time operational rain gauge quality-control tools in NWS hydrologic operations. *20th Conf. on Hydrology*, Boston, MA, Amer. Meteor. Soc., P2.4. [Available online at https://ams.confex.com/ams/Annual2006/techprogram/paper_102834.htm.]

Lakshmanan, V., T. Smith, K. Hondl, G. J. Stumpf, and A. Witt, 2006: A real-time, three-dimensional, rapid updating, heterogeneous radar merger technique for reflectivity, velocity, and derived products. *Wea. Forecasting*, **21**, 802–823, doi:10.1175/WAF942.1.

Larson, L. W., and E. L. Peck, 1974: Accuracy of precipitation measurements for hydrologic modeling. *Water Resour. Res.*, **10**, 857–863, doi:10.1029/WR010i004p00857.

Lauri, T., J. Koistinen, and D. Moisseev, 2012: Advection-based adjustment of radar measurements. *Mon. Wea. Rev.*, **140**, 1014–1022, doi:10.1175/MWR-D-11-00045.1.

Martinaitis, S. M., 2008: Effects of multi-sensor radar and rain gauge data on hydrologic modeling in relatively flat terrain. M. S. thesis, Department of Earth, Ocean and Atmospheric Sciences, Florida State University, 99 pp. [Available online at http://diginole.lib.fsu.edu/etd/2696.]

Marzen, J., and H. E. Fuelberg, 2005: Developing a high resolution precipitation dataset for Florida hydrologic studies. *19th Conf. on Hydrology*, New Orleans, LA, Amer. Meteor. Soc., J9.2. [Available online at https://ams.confex.com/ams/Annual2005/techprogram/paper_83718.htm.]

Matsuo, T., and Y. Sasyo, 1981: Non-melting phenomena of snowflakes observed in subsaturated air below freezing level. *J. Meteor. Soc. Japan*, **59**, 26–32.

Metcalfe, J. R., and B. E. Goodison, 1992: Automation of winter precipitation estimates: The Canadian experience. *Proc. WMO Technical Conf. on Instruments and Methods of Observations*, WMO/TD-462, Vienna, Austria, WMO, 81–85.

——, and ——, 1993: Correction of Canadian winter precipitation data. *Proc. Eighth Symp. on Meteorological Observations and Instrumentation*, Anaheim, CA, Amer. Meteor. Soc., 338–343.

Nitu, R., and K. Wong, 2010: CIMO survey on national summaries of methods and instruments for solid precipitation measurement at automatic weather stations. WMO Instruments and Observing Methods Rep. 102, WMO/TD-1544, 57 pp. [Available online at http://www.wmo.int/pages/prog/www/IMOP/publications/IOM-102_SolidPrecip.pdf.]

Parsons, D. A., 1941: Calibration of a Weather Bureau tipping-bucket gage. *Mon. Wea. Rev.*, **69**, 205–208, doi:10.1175/1520-0493(1941)069<0205:COAWBT>2.0.CO;2.

Passarelli, R. E., Jr., 1978: A theoretical explanation for *Z–R* relationships in snow. Preprints, *18th Conf. on Radar Meteorology*, Atlanta, GA, Amer. Meteor. Soc., 332–335.

Rasmussen, R., M. Dixon, S. Vasiloff, F. Hage, S. Knight, J. Vivekanandan, and M. Xu, 2003: Snow nowcasting using a real-time correlation of radar reflectivity with snow gauge accumulation. *J. Appl. Meteor.*, **42**, 20–36, doi:10.1175/1520-0450(2003)042<0020:SNUART>2.0.CO;2.

——, and Coauthors, 2012: How well are we measuring snow: The NOAA/FAA/NCAR winter precipitation test bed. *Bull. Amer. Meteor. Soc.*, **93**, 811–829, doi:10.1175/BAMS-D-11-00052.1.

Savina, M., B. Schäppi, P. Molnar, P. Burlando, and B. Sevruk, 2012: Comparison of a tipping-bucket and electronic weighing precipitation gauge for snowfall. *Atmos. Res.*, **103**, 45–51, doi:10.1016/j.atmosres.2011.06.010.

Sevruk, B., 1989: Wind induced measurement error for high-intensity rains. *Proc. Int. Workshop on Precipitation Measurement*, WMO Tech. Doc. 328, Geneva, Switzerland, WMO, 199–204.

——, 2005: Rainfall measurement: Gauges. *Encyclopedia of Hydrological Sciences*, M. G. Anderson, Ed., John Wiley and Sons, 529–536.

——, J.-A. Hertig, and R. Spiess, 1991: The effect of precipitation gauge orifice rim on the wind field deformation as investigated in a wind tunnel. *Atmos. Environ.*, **25A**, 1173–1179, doi:10.1016/0960-1686(91)90228-Y.

Sieck, L. C., S. J. Burges, and M. Steiner, 2007: Challenges in obtaining reliable measurements of point rainfall. *Water Resour. Res.*, **43**, W01420, doi:10.1029/2005WR004519.

Smith, C. J., 1986: The reduction of errors caused by bright bands in quantitative rainfall measurements made using radar. *J. Atmos. Oceanic Technol.*, **3**, 129–141, doi:10.1175/1520-0426(1986)003<0129:TROECB>2.0.CO;2.

Smith, J. A., D. J. Seo, M. L. Baeck, and M. D. Hudlow, 1996: An intercomparison study of NEXRAD precipitation estimates. *Water Resour. Res.*, **32**, 2035–2046, doi:10.1029/96WR00270.

Steiner, M., J. A. Smith, S. J. Burges, C. V. Alonso, and R. W. Darden, 1999: Effect of bias adjustment and rain gauge data quality control on radar rainfall estimation. *Water Resour. Res.*, **35**, 2487–2503, doi:10.1029/1999WR900142.

Thériault, J. M., R. Rasmussen, K. Ikeda, and S. Landolt, 2012: Dependence of snow gauge collection efficiency on snowflake characteristics. *J. Appl. Meteor. Climatol.*, **51**, 745–762, doi:10.1175/JAMC-D-11-0116.1.

VanCleve, D. D., Jr., and H. E. Fuelberg, 2007: An intercomparison between mean areal precipitation from gauges and a multisensor procedure. *21st Conf. on Hydrology*, San Antonio, TX, Amer. Meteor. Soc., 2.5. [Available online at https://ams.confex.com/ams/87ANNUAL/techprogram/paper_120249.htm.]

White, S. G., L. J. Winans, and J. V. Fiore, 2004: Development of the all-weather precipitation accumulation gauge for ASOS. Preprints, *Eighth Symp. on Integrated Observing and Assimilation Systems for Atmosphere, Oceans, and Land Surface*, Seattle, WA, Amer. Meteor. Soc., 7.3. [Available online at http://ams.confex.com/ams/pdfpapers/69273.pdf.]

Wilson, J. W., and E. A. Brandes, 1979: Radar measurement of rainfall: A summary. *Bull. Amer. Meteor. Soc.*, **60**, 1048–1058, doi:10.1175/1520-0477(1979)060<1048:RMORS>2.0.CO;2.

Yang, D., B. E. Goodison, J. R. Metcalfe, V. S. Golubev, R. Bataes, T. Pangburn, and C. L. Hanson, 1998: Accuracy of NWS 8″ standard nonrecording precipitation gauge: Results and application of WMO intercomparison. *J. Atmos. Oceanic Technol.*, **15**, 54–68, doi:10.1175/1520-0426(1998)015<0054:AONSNP>2.0.CO;2.

Young, C. B., B. R. Nelson, A. A. Bradley, J. A. Smith, C. D. Peters-Lidard, A. Kruger, and M. L. Baeck, 1999: An evaluation of NEXRAD precipitation estimates in complex terrain. *J. Geophys. Res.*, **104**, 19 691–19 703, doi:10.1029/1999JD900123.

——, A. A. Bradley, W. F. Krajewski, A. Kruger, and M. L. Morrissey, 2000: Evaluating NEXRAD multisensor precipitation estimates for operational hydrologic forecasting. *J. Hydrometeor.*, **1**, 241–254, doi:10.1175/1525-7541(2000)001<0241:ENMPEF>2.0.CO;2.

Zhang, J., K. Howard, and J. J. Gourley, 2005: Constructing three-dimensional multiple radar reflectivity mosaics: Examples of convective storms and stratiform rain echoes. *J. Atmos. Oceanic Technol.*, **22**, 30–42, doi:10.1175/JTECH-1689.1.

——, and Coauthors, 2011: National Mosaic and Multi-Sensor QPE (NMQ) system: Description, results, and future plans. *Bull. Amer. Meteor. Soc.*, **92**, 1321–1338, doi:10.1175/2011BAMS-D-11-00047.1.

——, Y. Qi, K. Howard, C. Langston, and B. Kaney, 2012: Radar quality index (RQI)—A combined measure of beam blockage and VPR effects in a national network. *Weather Radar and Hydrology*, R. J. Moore, S. J. Cole, and A. J. Illingworth, Eds., International Association of Hydrological Science, 388–393.